Incorporating spatial heterogeneity created by permafrost thaw into a landscape carbon estimate

E. F. Belshe,[1] E. A. G. Schuur,[1] B. M. Bolker,[2] and R. Bracho[1]

[1] The future carbon balance of high-latitude ecosystems is dependent on the sensitivity of biological processes (photosynthesis and respiration) to the physical changes occurring with permafrost thaw. Predicting C exchange in these ecosystems is difficult because the thawing of permafrost is a heterogeneous process that creates a complex landscape. We measured net ecosystem exchange of C using eddy covariance (EC) in a tundra landscape visibly undergoing thaw during two 6 month campaigns in 2008 and 2009. We developed a spatially explicit quantitative metric of permafrost thaw based on variation in microtopography and incorporated it into an EC carbon flux estimate using a generalized additive model (GAM). This model allowed us to make predictions about C exchange for the landscape as a whole and for specific landscape patches throughout the continuum of permafrost thaw and ground subsidence. During June through November 2008, the GAM predicted that the landscape on average took up 337.1 g C m^{-2} via photosynthesis and released 289.5 g C m^{-2} via respiration, resulting in a net C gain of 47.5 g C m^{-2} by the tundra ecosystem. During April through October 2009, the landscape on average took up 498.7 g C m^{-2} and released 410.3 g C m^{-2}, resulting in a net C gain of 87.8 g C m^{-2}. On average, between the years, areas with the highest permafrost thaw and ground subsidence photosynthesized 17.7% more and respired 3.3% more C than the average landscape. Areas with the least thaw and subsidence photosynthesized 15% less and respired 5.1% less than the landscape on average. By incorporating spatial variation into the EC C estimate, we were able to estimate the C balance of a heterogeneous landscape and determine the collective effect of permafrost thaw on the plant and soil processes that drive ecosystem C flux. In these study years, permafrost thaw appeared to increase the amplitude of the C cycle by stimulating both C release and sequestration, while the ecosystem remained a C sink at the landscape scale.

1. Introduction

[2] Northern high latitudes are disproportionally warming and arctic temperatures are predicted to increase by 6.5°C or more by the year 2100 in response to radiative forcing caused by increasing greenhouse gases and changes in albedo [*Chapin et al.*, 2000, 2005; *Hinzman et al.*, 2005; *Intergovenmental Panel on Climate Change*, 2007]. Currently, permafrost occurs within 24% of the ice-free land area in the northern hemisphere [*Zhang et al.*, 1999], and it is estimated 25%–90% will degrade into seasonally frozen ground by the year 2100 [*Anisimov and Nelson*, 1996;

Lawrence et al., 2008; *Saito et al.*, 2007]. According to recent estimates, permafrost soils contain twice as much carbon (1672 Pg) as the entire atmospheric pool [*Schuur et al.*, 2008; *Tarnocai et al.*, 2009]. If a portion of this C is released to the atmosphere it could result in a strong positive feedback to climate change. Understanding how permafrost thaw affects the rate of C exchange from this large pool is essential for understanding the global C cycle in a warmer world.

[3] Thawing of permafrost is a temporally dynamic and spatially heterogeneous process. Rising temperatures increase active layer (seasonally thawed surface layer) thickness and form thermokarst [*Jorgenson and Osterkamp*, 2005; *Zhang et al.*, 2005]. Thermokarst is uneven ground that forms when ice-rich permafrost thaws, drainage occurs, and the ground surface subsides [*Jorgenson and Osterkamp*, 2005]. These localized changes in surface relief greatly alter the surface hydrology of the area. As water is redistributed from higher to lower microtopographical areas, thermal erosion by the

[1]Department of Biology, University of Florida, Gainesville, Florida, USA.
[2]Department of Mathematics and Statistics, McMaster University, Hamilton, Ontario, Canada.

movement of water warms the soil and further perpetuates permafrost thawing [*Kane et al.*, 2001; *Osterkamp et al.*, 2009]. This positive feedback creates a mosaic of patches that range from high, dry embankments with shallow active layers to subsided areas with relatively wet, warm soils and deep active layers [*Lee et al.*, 2011; *Osterkamp et al.*, 2009; *Vogel et al.*, 2009]. Furthermore, this pattern of ground subsidence, dictated by the initial presence of ice-rich permafrost, is interspersed throughout the landscape and ultimately creates a mosaic of various degrees of permafrost thaw and microtopography.

[4] The future C balance of high-latitude ecosystems depends on the sensitivity of biological processes (photosynthesis and respiration) to the physical changes in temperature and moisture occurring with permafrost thaw. But, predicting C exchange in these ecosystems is difficult because of the landscape heterogeneity created as permafrost thaws. Since adjacent patches can have very different physical environments, they can have very different gross primary production (GPP) and ecosystem respiration (R_{eco}) [*Lee et al.*, 2011; *Vogel et al.*, 2009]. Landscape-scale GPP and R_{eco} will depend on the cumulative response of the landscape to permafrost thaw, which in turn will dictate the direction and magnitude of net ecosystem exchange (NEE = GPP − R_{eco}).

[5] The response of the C cycle to spatial and temporal environmental variation is often nonlinear and not simply described by the mean response [*Aubinet et al.*, 2002]. Therefore, an appropriate understanding of both the spatial and temporal variation of C flux is essential for estimating the C balance of a landscape. But the intensive temporal sampling required for good estimates of C flux makes it difficult to obtain extensive, spatially explicit C flux data. Eddy covariance (EC) provides a method to directly measure C exchange at a high level of temporal resolution over a large spatial scale [*Baldocchi*, 2003]. But fluxes measured by EC are commonly assumed to come from a homogenous surface, which makes it difficult to resolve the cumulative contribution of localized features in the landscape to an EC estimate [*Laine et al.*, 2006; *Schmid and Lloyd*, 1999]. Although much effort has gone into developing and using models to locate where fluxes originate (i.e., the footprint of an EC tower) [*Kormann and Meixner*, 2001; *Schmid*, 1997, 2002; *Schmid and Lloyd*, 1999], less effort has gone into incorporating spatial information back into EC C estimates. However, the abundance of data produced by EC towers gives us the ability to explore spatial patterns of C flux.

[6] In this study, we use generalized additive models (GAMs) to generate a continuous time series of NEE for a tundra landscape undergoing permafrost thaw. We developed a spatially explicit quantitative metric of permafrost thaw based on variation in microtopography. By incorporating our spatial metric into EC gap-filling models, we were able to make C flux predictions for the landscape as a whole, as well as for specific landscape patches throughout the continuum of permafrost thaw and ground subsidence. We tested the robustness of our models against more widely used (nonspatial) gap-filling methods. Our objectives were to more accurately estimate the C balance of a heterogeneous landscape and to explore the collective effect of permafrost thaw on the plant and soil processes that dictate ecosystem C exchange.

2. Material and Methods

2.1. Site Description

[7] The study site is within the Eight Mile Lake (63°52′42′ N, 149°15′12′W), watershed in the northern foothills of the Alaska Range near Denali National Park and Preserve [*Schuur et al.*, 2007, 2009]. This upland area occurs within a vulnerable band of discontinuous permafrost near the point of thaw due to the combination of its elevation and geographic position [*Romanovsky et al.*, 2007; *Yocum et al.*, 2006]. Deep permafrost temperature has been measured at the site since 1985 and during this time thermokarst terrain has developed and expanded as the permafrost has warmed [*Osterkamp et al.*, 2009]. Vegetation at the site is dominated by moist acidic tussock tundra comprising sedge (*Eriophorum vaginatum*), deciduous and evergreen shrubs (*Vaccinium uliginosum, Rubus chamaemorus, Betula nana,* and *Ledum palustre*), and nonvascular plants (*Sphagnum* spp., *Dicranum* spp., feathermoss, and lichens). Soils at the site are classified as Gelisols because permafrost is found within 1 m of the soil surface [*Soil Survey Staff*, 1999]. An organic horizon, 0.45–0.65 m thick, covers cryoturbated mineral soil that is a mixture of glacial till (small stones and cobbles) and windblown loess. Organic C pools in the top meter of soil range between 55 and 69 kg C m^{-2} [*Hicks Pries et al.*, 2011].

[8] The long-term mean annual air temperature (1976–2009) of the area is −1.0°C and the growing season (May–September) mean air temperature is 11.2°C, with monthly averages ranging from −16°C in December to +15°C in July. The long-term annual mean precipitation is 378 mm with a growing season mean precipitation of 245 mm (National Climatic Data Center, National Oceanic and Atmospheric Administration). Mean growing season air temperature was 8.1°C and 9.7°C during 2008 and 2009, respectively, and growing season precipitation was 346 mm and 178 mm during 2008 and 2009, respectively.

2.2. Eddy Covariance Measurements

[9] NEE was measured using eddy covariance (EC) from June to December 2008 and April to October 2009. The EC system consisted of a CSAT3 sonic anemometer (Campbell Scientific, Logan, Utah) and an open path CO_2/H_2O gas analyzer (Li-7500, LI-COR Biosciences, Lincoln, Nebraska) mounted on a 2 m tower. Data were recorded at a frequency of 10 Hz on a CR5000 data logger (Campbell Scientific), and fluxes were Reynolds averaged over 30 min time periods [*Reynolds*, 1895]. Calibration was preformed monthly during the growing season using a zero CO_2 air source, a ±1% standard CO_2 concentration, and a dew point generator (Li-610, LI-COR Biosciences) for water vapor. The EC tower was placed within a patchy landscape consisting of visibly subsided areas to the North and West and relatively even terrain to the South and East. The fetch from the tower was greater than 300 m in all directions and winds predominantly came from the NE and SW. An analytical footprint model developed by *Kormann and Meixner* [2001] showed on average 50% of fluxes originated within the first

50 m around the tower, and greater than 80% of fluxes originated within 200 m from the tower.

2.2.1. EC Data Handling

[10] Raw CO_2 fluxes were corrected for damping of high-frequency fluctuations, sensor separation, and misalignment of wind sensors with respect to the local streamline [*Aubinet et al.*, 1999; *Moncrieff et al.*, 1997; *Wilczak et al.*, 2001]. CO_2 fluxes were then corrected for variations in air density due to fluctuation in water vapor and heat fluxes [*Webb et al.*, 1980] and for fluctuations caused by surface heat exchange from the open path sensor during wintertime conditions [*Burba et al.*, 2008]. Data screening was applied to eliminate half-hourly fluxes with systematic errors and nonrelevant environmental influences such as (1) incomplete half-hour data sets as a result of system calibration or maintenance; (2) time periods when the canopy was poorly coupled with the external atmospheric conditions as defined by the friction velocity, u^* (threshold <0.12 m s^{-1}) [*Clark et al.*, 1999; *Goulden et al.*, 1996]; and (3) excessive variation from the half-hourly mean based on an analysis of standard deviations for u, v, and w wind statistics and CO_2 fluxes. Fluxes were then divided into weekly data sets for both day and night conditions and unrealistic low or high values (>2 standard deviations from the mean) were filtered out. In total, ecosystem fluxes were measured 72% and 96% of the time during the 2008 and 2009 campaigns, respectively, while 64% and 60% of those values were eliminated by the screening criteria listed above. The quality of our data was evaluated by the degree of growing season energy closure ($R_{net} = LE + H + G$), which was 76% in 2008 and 73% in 2009. Ground heat flux (G) was estimated as the change in soil temperature with depth plus soil heat storage [*Liebethal et al.*, 2005; *Liebethal and Foken*, 2007]. To calculate soil heat storage, we assumed 40% organic matter content [*Hicks Pries et al.*, 2011] and 60% volumetric water content based on soil cores taken from the site. Measurements of half-hour NEE were calculated as: NEE = $Fco2$ + Fs, where F_{CO2} was the mean flux of CO_2 at measurement height and F_s was the half-hour change in CO_2 stored below measurement height. Because of the short vegetation ($\sim$30 cm), we calculated the change in CO_2 storage by taking the difference in successive CO_2 measurements at the measurement height [*Hollinger et al.*, 1994]. We used the meteorological convention that positive NEE represents a transfer of CO_2 from the ecosystem to the atmosphere.

2.2.2. Environmental Measurements

[11] Standard meteorological data were collected on a tower adjacent to the EC tower, including photosynthetic photon flux density (PPFD; Li-190SA, LI-COR Biosciences), incident radiation (Li-200SA, LI-COR Biosciences), net radiation (REBS Q*7.1, REBS Inc., Seattle, Washington), relative humidity and air temperature (Vaisala HMP45c, Campbell Scientific), and wind speed and direction (RM Young 3001, Campbell Scientific). Soil temperature profiles (5, 10, 15, 20, and 25 cm from surface) were measured with constantan-copper thermocouples and a thermistor (at 5 cm depth only; 107, Campbell Scientific). Moisture integrated over the top $\sim$15 cm of soil was measured with a Campbell CS615 water content reflectometer. All measurements were recorded at half-hour average intervals with a CR5000 data logger (Campbell Scientific). A complete replicate set of

micrometerological measurements were collected at a tower 100 m to the NW of EC tower, and were used to interpolate gaps in micrometeorological data measured at the EC tower.

2.3. Landscape Properties

[12] To quantify the amount and distribution of land surface subsidence associated with permafrost thaw, a digital elevation model (DEM) was created from point measurements of elevation. Fine-scale differences in elevation were measured with a high-resolution differential global position system (dGPS). One GPS unit (Trimble 5400) was placed at a nearby USGS geodetic marker (WGS84, 63°53′16.56″N, 149°14′17.92″W), which acted as the reference receiver. Using a second GPS unit (Trimble 5400) secured to a backpack, a kinematic survey was conducted by walking transects within a 400 m diameter circle encompassing the EC tower footprint. Geographic position and elevation were collected at 5 s intervals, yielding a total of 7220 points. These data were postprocessed with methodology developed by UNAVCO using Trimble Geomatics Office (Dayton, Ohio).

[13] To create the DEM of the area surrounding the EC tower, spherical models were fit to empirical semivariograms, and ordinary kriging was used to interpolate between point measurements using the calculated range of 282 m, a nugget of 0.02, and a partial sill of 0.47. Variogram analysis and kriging was done with the Geostatistical analyst extension in ArcGIS 9.3. Because the study site is on a gentle slope ($\sim$5%), the original DEM was corrected for overall slope elevation changes, so we could decipher small-scale subsidence features. To correct for the slope, the DEM was first rescaled so the minimum elevation equaled zero. Mean elevation within 30 m blocks was subtracted from the rescaled DEM, resulting in the deviation in elevation away from the mean plane. This created a map of small-scale variations in topography that we define here as microtopography. Pixel resampling and calculations were done using the aggregate function, resample tool, and the raster calculator in the Spatial Analyst extension in ArcGIS 9.3.

[14] To obtain landscape information in a form comparable to EC data, we extracted information on microtopography corresponding to each wind direction sampled by the EC tower. Virtual transects 200 m in length, originating at the EC tower and radiating out in every wind direction (0–359), were created. A distance of 200 m was chosen because it corresponded to the distance where on average $>80\%$ of scalar fluxes originated based on an analytical footprint model [*Kormann and Meixner*, 2001]. Microtopography (i.e., local elevation) was sampled every meter along each transect using Hawth's Analysis Tools (H. L. Beyer, Hawth's Analysis Tools for ArcGIS, http://www.spatialecology.com/htools/tooldesc.php, 2004) in ArcGIS 9.3. The standard deviation of microtopography, which we refer to as roughness, was calculated for each transect (wind direction). This calculated metric was chosen because it captures the variation in microtopography created by permafrost thaw (both subsided areas and raised embankments). Our metric, roughness, should not be confused with the micrometeorological term roughness length.

[15] To calculate our metric, roughness, corresponding to each (half-hour) flux measurement, we simply calculated the standard deviation of the per meter values of microtopography

along the entire transect corresponding to the measured wind direction. We acknowledge that C fluxes measured over a 30 min period do not emanate from a one-dimensional transect; instead they come from two-dimensional areas in the landscape. To find the best spatial metric corresponding to the measured C flux, we also calculated roughness for the three and five adjacent transects of the measured wind direction. We found no change in the relationship between C flux and roughness when using a greater number of transects. Also, in principle, footprint models provide more information than the overall radial scale of the area surrounding the EC tower because they help to pinpoint where in the landscape fluxes are originating [*Kormann and Meixner*, 2001; *Schmid*, 1997, 2002; *Schmid and Lloyd*, 1999]. So, for comparison, we also used estimates of the cumulative probability of fluxes coming from different fetches, calculated by a footprint model, to calculate a weighted standard deviation of roughness. However, we chose to use the simple nonweighted roughness because under certain conditions weighting caused relatively flat areas to the SE to have a higher standard deviation than the most subsided areas to the NW. We believe this discrepancy is due to the mismatch in scale between our one-dimensional transects and the two-dimensional cumulative density function calculated by the footprint model [*Kljun et al.*, 2003; *Kormann and Meixner*, 2001].

[16] We explored the relationship between roughness and normalized difference vegetation index (NDVI), and the relationship between microtopography and active layer depth (ALD). NDVI was calculated using spectral data from an IKONOS image of the site acquired in June 2008. Mean NDVI was calculated for each of the 360 virtual transects radiating out from the EC tower, and was compared to the roughness of the corresponding transect. ALD was measured at 310 locations stratified at various distances within the potential EC footprint, by measuring the length of a metal probe inserted into the soil until the impenetrable frozen layer was reached. The geographic location of each site was measured and subsequently used to extract corresponding values of elevation from the map of microtopography. We only compared ALD to microtopography because we did not have a continuous surface of ALD; therefore, were unable to extract data for the 360 virtual transects to compare with roughness. Relationships were explored with generalized additive models using the mgcv package in R [*R Development Core Team*, 2010; *Wood*, 2008].

2.4. Estimation of Landscape-Scale Carbon Exchange

[17] To estimate the carbon balance of an ecosystem, measured CO_2 fluxes must be gap filled to generate a continuous time series of net ecosystem exchange (NEE). We estimated carbon exchange using two gap-filling strategies: (1) a novel gap-filling strategy using generalized additive models (GAMs) that are flexible enough to incorporate spatial information and (2) nonlinear (NL) relationships with nonspatial environmental variables.

[18] Although NEE is directly measured by the EC technique, the driving force of the exchange is dependent on environmental conditions. Therefore, we modeled NEE for gap filling during winter, growing season (GS) days, and GS nights separately. The beginning and end of the GS was determined by abrupt changes in net radiation corresponding to snowmelt and widespread snow cover,

respectively. Generally, the GS began in early May and ended at the end of September. Data during the GS were split into day and night by ambient light, so when PPFD was greater than 10 μmol m^{-2} s^{-1} daytime conditions were assumed. During daytime, NEE is the balance between gross primary production (GPP) and ecosystem respiration (R_{eco}). To tease apart their contributions, we modeled R_{eco} during GS days using models fitted with GS night data and calculated GPP as the difference between NEE and R_{eco} (GPP = NEE $-$ R_{eco}). Once soil temperature at 5 cm fell below 0°C, winter conditions were assumed. During these conditions, photosynthesis is not occurring so NEE is equivalent to R_{eco}.

2.4.1. Gap-Filling Strategy 1: Generalized Additive Models

[19] To generate a continuous time series, we gap filled NEE using generalized additive models (GAMs), an extension of generalized linear models where a response is modeled as the additive sum of smoothed covariate functions [*Hastie and Tibshirani*, 1990; *Wood*, 2006]. With GAMs, nonlinear effects can be modeled without manually specifying the shape of the relationships, which provided us the flexibility to incorporate roughness along with other explanatory variables into the prediction of NEE [*Wood*, 2006; *Zuur et al.*, 2009]. To control the shape of functions, we used penalized regression splines, which determine the appropriate degree of smoothness of each smoothing function by generalized cross validation (GCV) and adds a "wiggliness" penalty when estimating the coefficients of each smooth with maximum likelihood [*Wood*, 2006]. All GAMs used had the basic form

$$y_i = \beta_0 + f_1(x_i) + f_2(z_i) + f_3(x_i, z_i) + \varepsilon_i, \qquad (1)$$

where y_i denotes the response variable (NEE or R_{eco}), β_0 is the intercept, functions $f_1(x_i)$ and $f_2(z_i)$ are smooth functions of explanatory variables x_i and z_i, and $f_3(x_i, z_i)$ is a two-dimensional smooth function of their interactions. We used thin plate regression splines as the basis for representing smooths (f_1 and f_2) for single covariates and tensor product smooths (f_3) for interactions (multiple covariates) because they have been found to perform better when covariates are not on the same scale [*Wood*, 2006]. We forced the effective degrees of freedom in each model to count as 1.4 degrees of freedom in the GCV score, which forces the model to be slightly smoother than it might otherwise be, this is an ad hoc way to avoiding overfitting [*Kim and Gu*, 2004].

[20] Because eddy covariance data are heteroscedastic [*Richardson et al.*, 2008] and there were distinct patterns in the residuals, we fit GAMs using a mixed model framework (GAMM) with a Gaussian error distribution to facilitate the incorporation of an exponential variance structure:

$$\varepsilon_i \sim N\left(0, \sigma^2 \cdot e^V\right), \qquad (2)$$

where the variance of the residuals σ^2 is multiplied by an exponential function of the fitted values (V). We used all data in a single dummy group as our random effect to facilitate the incorporation of the variance structure into the GAM [*Dormann*, 2007; *Wood*, 2006; *Zuur et al.*, 2009]. All models were fitted using the mgcv package [*Wood*, 2006] in R [*R Development Core Team*, 2010].

[21] A subset of explanatory variables was selected a priori including: PPFD, temperature (air, soil at 5 cm, depth-integrated soil temperature down to 25 cm), roughness, and day of year (DOY). We suspected there might be complex interactions between explanatory variables, so both direct effects and all possible interactions were compared. Models were selected for each time period (winter, GS day, GS night) during each year (2008, 2009), by starting with the full model containing all variables and interactions and using a form of automatic backward selection in which the penalization term for each smooth could automatically set the term to zero and remove it from the model as appropriate [*Wood*, 2008]. We also took into consideration how removing terms affected (1) the GCV score (the lower the better), (2) the deviance explained (the higher the better), and (3) the Akaike Information Criterion (AIC, the lower the better) [*Anderson et al.*, 1998, 2001].

[22] Because our GAM models incorporated landscape information, they allowed us to estimate the landscapes carbon balance in two different ways. If we assumed the landscape was one unit (measurements taken from one "population" of fluxes), then gaps in the time series were filled depending on the measured wind direction at the time of the gap. This resulted in a single time series of carbon exchange for the landscape (GAM 1). Alternately, if we assumed the landscape was a combination of multiple patches (wind directions), all absorbing or releasing C simultaneously, then each wind direction was gap filled separately for the entire time series. This resulted in 360 separate time series, whose predictions were averaged to achieve an estimate of carbon exchange for the entire landscape (GAM 360). This method allowed us to estimate C exchange for the entire heterogeneous landscape and made it possible to compare predictions from landscape patches that differed in roughness. Both methods of prediction were done for each time period during 2008 and 2009.

2.4.2. Gap-Filling Strategy 2: Nonlinear Regressions

[23] For comparison we also gap-filled data using a more traditional nonlinear (NL) regression approach. During GS days, gaps were filled using parameters obtained by fitting half-hour NEE to PPFD using a nonrectangular hyperbola [*Thornley and Johnson*, 1990]:

$$\text{NEE} = ((\alpha \cdot \text{PPFD} \cdot P_{max})/(\alpha \cdot \text{PPFD} + P_{max})) - R, \quad (3)$$

where α is the linear portion of the light response curve, PPFD is photosynthetically active radiation, P_{max} is the asymptote, and R is the intercept or dark respiration term. To capture changes in phenology, parameters were estimated biweekly or monthly depending on the variation among weeks. We incorporated an exponential variance structure due to the heteroscedacity of the data and used maximum likelihood to estimate parameters using the bbmle package (B. M. Bolker, bbmle: Tools for general maximum likelihood estimation, https://r-forge.r-project.org/R/?group_id=176, 2010) in *R*.

[24] We were unable to fit exponential models to winter and GS night data separately, so we gap filled with parameters estimated using both data together. Parameters were estimated using the following equation:

$$R_{eco} = \alpha \cdot e^{\beta \cdot T}, \quad (4)$$

where α is the intercept and β is the slope and T was depth-integrated soil temperature during 2008 and soil temperature measured at 5 cm during 2009. We compared models with various forms of temperature (air, soil at 5 cm, depth-integrated soil) and chose the best model based on AIC. We choose not to model average because the best model's AIC was much lower (>5 pts) than the alternatives. An exponential variance structure was added and parameters were estimated using generalized nonlinear least squares using the nlme package in R (J. Pinheiro et al.,, nlme: Linear and nonlinear mixed effects models, http://cran.r-project.org/web/packages/nlme/index.html, 2010).

2.4.3. Model Performance

[25] We compared the coefficient of variation (R^2) and Akaike Information Criterion (AIC [*Anderson et al.*, 1998, 2001]) of each GAM and NL model, during each time period. Because of the variation in model types, we calculated the R^2 simply as the correlation between the predicted values from each model and the observed values. To assess the predictive performance of the GAM and NL models, we performed cross validation. Ten percent of the data was randomly removed, models were fitted to the remaining data, and these models were then used to predict responses for the withdrawn ten percent. This process was repeated ten times and the root mean square error (RMSE) was calculated for each model. We then compared RMSE of the GAM and NL models within each time period using a *t* test at a statistical significance of $p < 0.05$. To calculate comparable values of AIC we used the following equation:

$$\text{AIC} = 2 \cdot n \cdot \log(\text{RMSE}) + 2 \cdot p, \quad (5)$$

where n is the number of observations and p is the number of parameters [*Venables and Ripley*, 2002].

3. Results

3.1. Landscape Heterogeneity of the EC Footprint

[26] Our map of microtopography captured the spatial pattern of ground subsidence created by permafrost thaw within the EML watershed (Figure 1). The largest variation in microtopography was found to the NW of the EC tower, while areas to the E and SE were relatively flat. This spatial distribution of ground subsidence agreed well with patterns visible in high-resolution aerial photographs of the site. In addition, the maximum (0.5 m) and minimum (−0.9 m) deviations away from the mean elevation were consistent with field measurements of the depth of individual subsided features and height of raised embankments created by thaw (data not shown). This pattern was mirrored by our calculated landscape metric roughness. Transects with the highest and lowest roughness corresponded with the winds coming from the N-NW and SW-SE, respectively (Figure 1).

[27] In general, the depth of the active layer increased as local elevation decreased (became more subsided) and microtopography explained 51% (adjusted $R^2 = 0.51$) of the observed variation in active layer depth. The relationship was nonlinear, with little variation in active layer depth at sites where elevation was positive or slightly negative, followed by an exponential increase in active layer depth as elevation fell below −0.2 m (Figure 2a). Transects with more variation in microtopography (high roughness) were

found to have higher mean NDVI than transects with less variation (low roughness), and roughness explained 55% of the variation in mean NDVI (adjusted $R^2 = 0.55$, effective degrees of freedom = 6.1). This relationship was also nonlinear, with NDVI linearly increasing with roughness, then
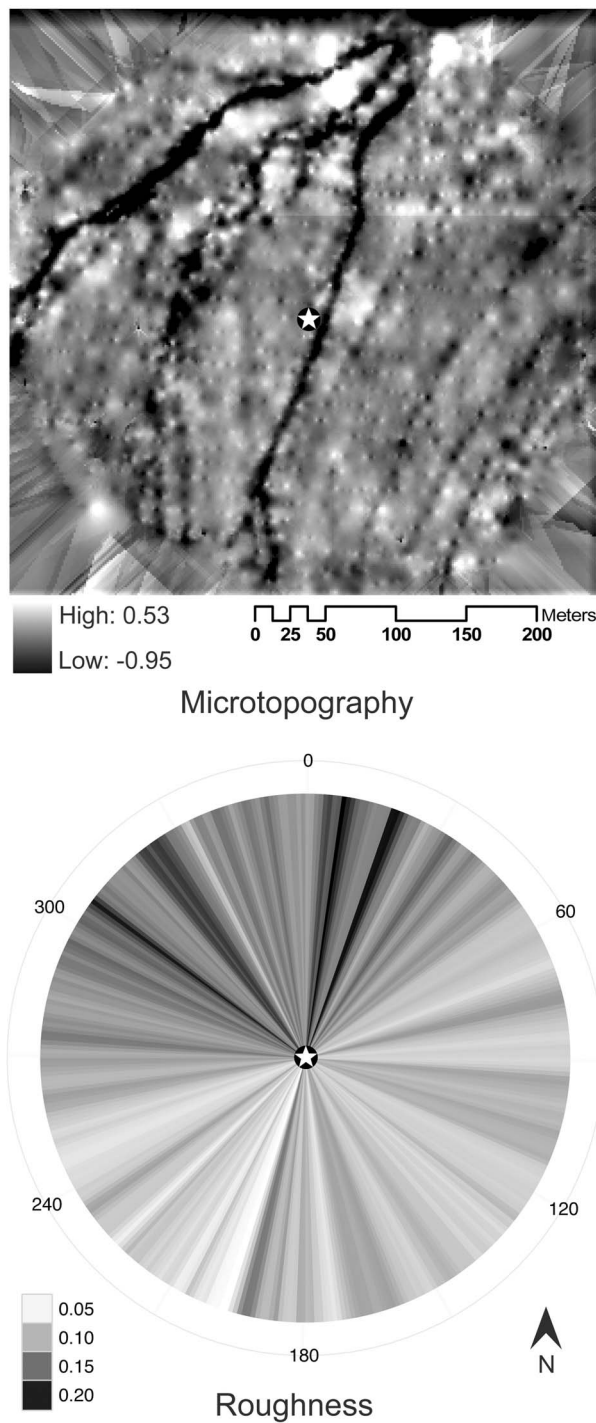
Figure 1. (top) Map of microtopography surrounding the eddy covariance (EC) tower (star), with lighter shades indicating areas where the ground surface is higher than the mean elevation of the landscape and darker shades indicating where the ground surface was lower than the mean elevation (i.e., subsided). (bottom) Transects numbering 360 radiating out from the EC tower (star) corresponding to the wind direction sample by the tower. The color of transects grades from light to dark as the degree of roughness increases. Note that in general, the roughest transects occur to the north and northwest of the EC tower, while transects to the south and east have lower roughness.

Figure 2. (a) Nonlinear relationship between active layer depth (ALD; cm) and microtopography (adjusted $R^2 = 0.51$) with 95% confidence intervals. Note the small amount of variation in ALD where microtopography is positive or slightly negative, then an exponential increase in ALD as microtopography falls below -0.2 m. (b) Nonlinear relationship between mean normalized difference vegetation index (NDVI) and roughness (adjusted $R^2 = 0.55$) with 95% confidence intervals. NDVI linearly increases until roughness reaches 0.14, then NDVI levels out or decreases.
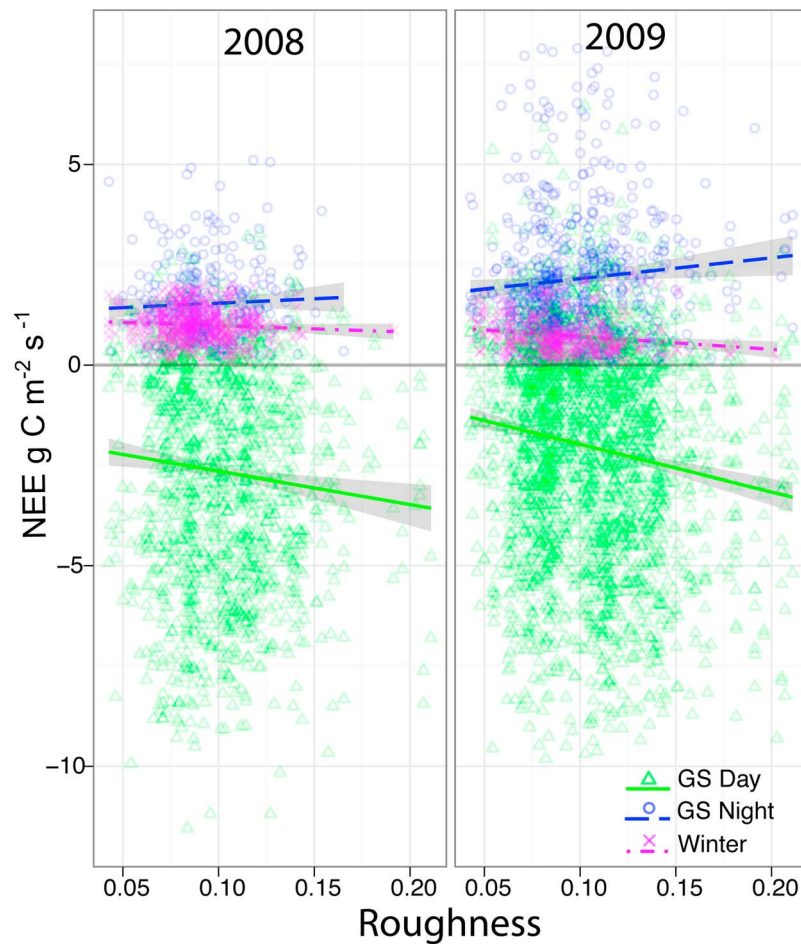
Figure 3. Relationships between roughness and net ecosystem exchange (g C m^{-2}) during growing season (GS) nights, GS day, and winter. Actual data points are displayed behind the trend lines.

leveling out and sometimes decreasing as roughness increased above 0.14 (Figure 2b).

[28] The magnitude of net ecosystem exchange (NEE) increased as the roughness of the landscape increased (Figure 3). During GS days, NEE became more negative (more C uptake) with increasing roughness. More C was released from areas with higher roughness during GS nights, but the trend of increased C emission with increasing roughness decreased in magnitude and then reversed during the winter months (Figure 3).

3.2. Model Performance

[29] GAM models outperformed the nonspatial NL models for gap-filling C exchange. GAM models had a higher or equivalent coefficient of determination (R^2) and higher predictive power (lower AIC) than NL models during every time period in both 2008 and 2009 (Table 1). During cross validation, GAM models always had lower mean RMSE, but were only significantly lower (at $p < 0.05$) during GS days of 2008 and 2009 (Table 1).

3.3. Predictions of Ecosystem C Balance

[30] In general, the three gap-filling methods (NL, GAM 1, GAM 360) resulted in similar estimates of NEE, GPP and

Table 1. Coefficient of Variation, Predictive Power, and Cross-Validation RMSE for Generalized Additive Model and Nonlinear Model During Growing Season Day, Growing Season Nights, and Winter 2008 and 2009[a]

Time Period	Model	R^2	Δ AIC	RMSE
2008				
GS-D	GAM	0.83	0	0.067 ± 0.03[b]
	NL	0.78	2458.6	0.161 ± 0.06
GS-N	GAM	0.26	0	0.132 ± 0.09
	NL	0.26	93.4	0.151 ± 0.10
Winter	GAM	0.16	0	0.047 ± 0.04
	NL	0.01	116.9	0.053 ± 0.05
2009				
GS-D	GAM	0.83	0	0.052 ± 0.02[b]
	NL	0.78	5971.8	0.181 ± 0.17
GS-N	GAM	0.29	0	0.085 ± 0.06
	NL	0.22	772.9	0.136 ± 0.09
Winter	GAM	0.22	0	0.041 ± 0.03
	NL	0.12	363.7	0.065 ± 0.06

[a]Abbreviations are as follows: GAM, generalized additive model; GS-D, growing season day; GS-N; growing season nights; NL, nonlinear model.
[b]Significantly different than model counterpart at p < 0.05.
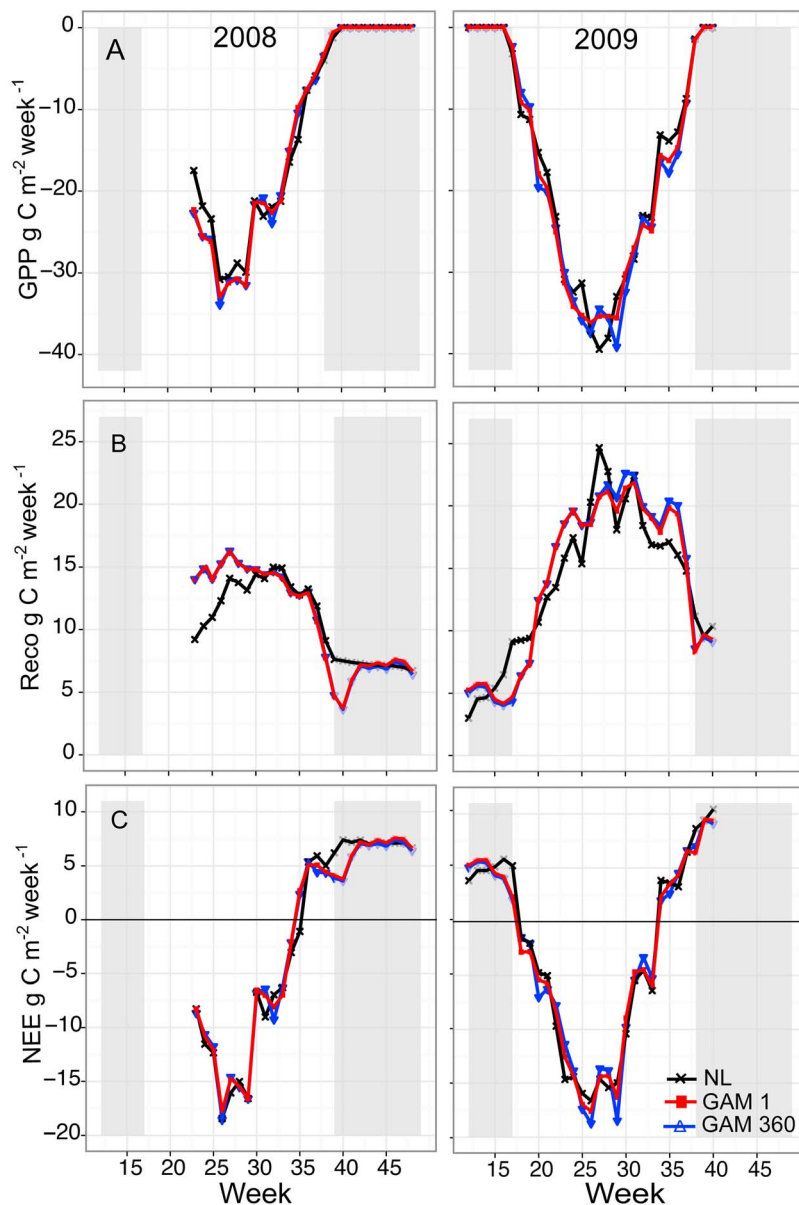
Figure 4. (a) Gross primary production (GPP; g C m^{-2}), (b) ecosystem respiration (R_{eco}; g C m^{-2}), and (c) net ecosystem exchange (NEE; g C m^{-2}) for the three methods of prediction, generalized additive model (GAM) 360, GAM 1, and nonlinear, over the measurement campaigns of 2008 and 2009. Shaded areas denote winter conditions, and negative values occur when the ecosystem is a C sink.

R_{eco} for the time periods 6 June through 8 December 2008 (weeks 24–48) and 24 April through 10 October 2009 (weeks 12–40; Figure 4). Weekly estimates of NEE, GPP and R_{eco} generated for both GAM methods closely mirror one another throughout both 2008 and 2009 (Figure 4). Although the NL and two GAM methods generated similar final estimates of net ecosystem exchange, there were some notable differences. The two GAM methods estimated a slightly higher uptake of carbon (more negative GPP) than their NL counterpart, 10–13 g C m^{-2} more in 2008 and 12–19 g C m^{-2} more in 2009. This difference in GPP was spread throughout the growing season, with no single week solely responsible for the difference (Figure 4a). Similarly, the two GAM methods estimated a slightly higher release of

carbon (R_{eco}) than the NL method, 10–11 g C m^{-2} more in 2008 and 7 – 13 g C m^{-2} more during 2009. Unlike GPP, however, differences in R_{eco} could be attributed to certain time periods. During 2008, the major differences between the predictions of the two methods occurred during the early growing season (weeks 21–29) where the NL method predicted lower R_{eco} than either GAM method. During the majority of the GS of 2009 the GAM methods estimated higher R_{eco} than the NL method. The other time of divergence among the methods was during transitions into and out of the growing season. The GAM methods predicted lower R_{eco} than the NL method during transition from GS to winter (weeks 39–40) in 2008 and during the transition from winter to GS (week 15–19) in 2009 (Figure 4b).
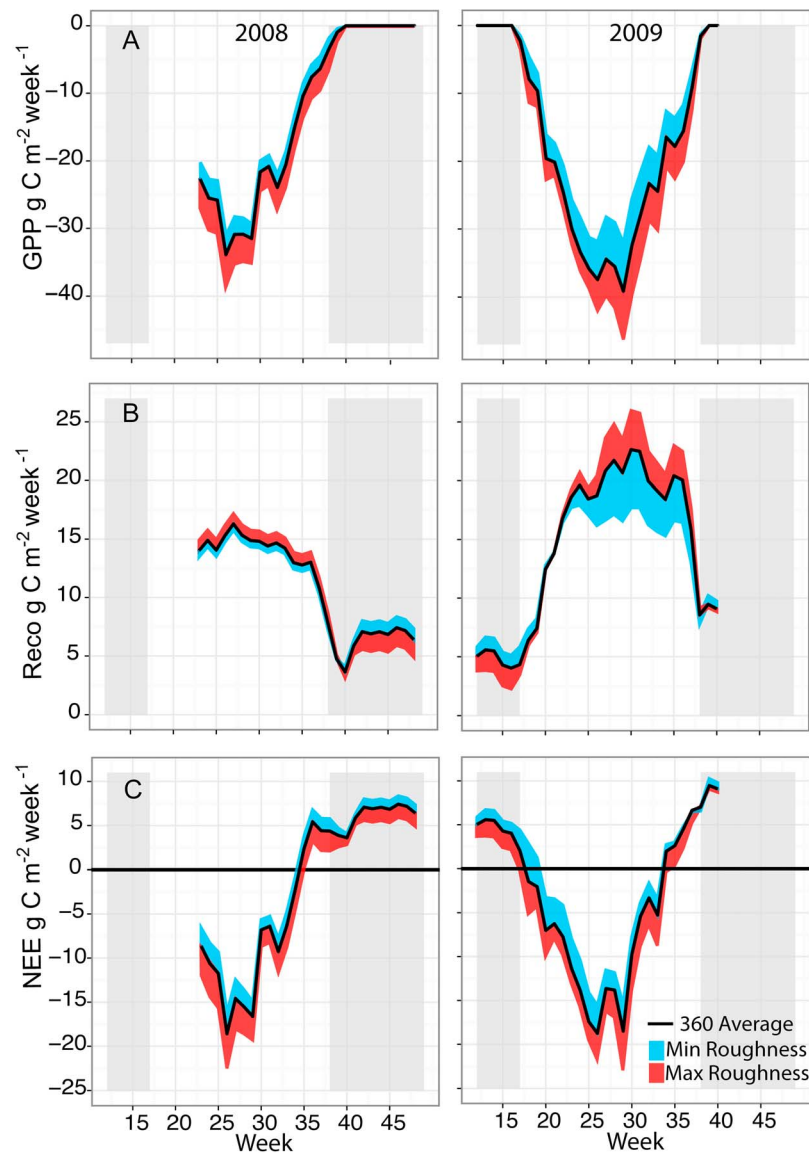
Figure 5. (a) GPP (g C m^{-2}), (b) R_{eco} (g C m^{-2}), and (c) NEE (g C m^{-2}) for the landscape on average (360 average) and for the wind direction with maximum roughness and minimum roughness over the measurement campaigns of 2008 and 2009. Shaded areas denote winter conditions, and negative values occur when the ecosystem is a sink.

3.4. Predictions of Landscape Heterogeneity of C Flux

[31] Using GAMs, we were also able to predict C exchange for each wind direction. To estimate the C balance for the entire landscape we calculated the mean carbon flux of all wind directions for each 30 min interval throughout 2008 and 2009 (GAM 360). This resulted in an estimate of NEE, GPP, and R_{eco} for the landscape on average but also allowed us to compare C fluxes from the wind directions with the minimum and maximum roughness to further understand the influence of permafrost thaw and ground subsidence on C flux.

[32] From June to December 2008, GAM 360 estimated the landscape on average took up 337.1 g C m^{-2} via photosynthesis and released 289.5 g C m^{-2} via respiration,

resulting in an ecosystem carbon gain of 47.5 g C m^{-2} (Figure 5 and Table 2). The direction with the maximum roughness had higher GPP and R_{eco} than the landscape on average, while the direction with the minimum roughness had lower GPP and R_{eco} (Figure 5 and Table 2). This resulted in the direction with maximum roughness gaining 55% more C than the landscape on average, while the direction with minimum roughness gained 76.4% less C (Table 2).

[33] From April to October 2009, the landscape on average took up 498.7 g C m^{-2} via photosynthesis and released 410.3 g C m^{-2} via respiration, resulting in a net gain of 87.8 g C m^{-2} (Figure 5 and Table 2). Again, the direction with the maximum roughness had higher GPP and R_{eco} than

Table 2. Carbon Estimates for the Wind Direction With the Minimum Roughness, Maximum Roughness, and the Average of All 360 Wind Directions During June to December 2008 and April to October 2009[a]

Roughness	2008			2009		
	GPP	R_{eco}	NEE	GPP	R_{eco}	NEE
Minimum	−300.3	288.3	−11.2	−403.6	386.6	−33.6
Maximum	−397.4	291.9	−106.1	−586.4	450.6	−149.8
Average	−337.1	289.5	−47.5	−498.7	410.3	−87.8

[a]Carbon estimates are in g C m^{-2}. Negative numbers denote when the ecosystem is taking up carbon. Abbreviations are as follows: GPP, gross primary production; R_{eco}, ecosystem respiration; NEE, net ecosystem exchange.

the landscape on average, while the direction with the minimum roughness had lower GPP and R_{eco} (Figure 5 and Table 2). This resulted in the direction with maximum roughness gaining 41.4% more C than the landscape on average, while the direction with minimum roughness gained 61.7% less C (Table 2).

[34] The amplified increase in GPP with maximum roughness was consistent throughout all weeks of the growing season in both 2008 and 2009 (Figure 5a). Unlike GPP, the increase in R_{eco} with roughness was not consistent throughout either year. During the GS of both years, the landscape with maximum roughness had higher R_{eco}, but during the winter this trend reversed and the landscape with min roughness had higher R_{eco} (Figure 5b). Even though areas with minimum roughness had higher R_{eco} during winter, the overall carbon emission throughout 2008 and 2009 was still greater from areas with maximum roughness (Table 2).

4. Discussion

4.1. Quantifying Spatial Heterogeneity

[35] Microtopography is an easy to obtain, integrative metric of the physical and biological changes occurring as the result of permafrost thaw within the EML watershed because it correlates with variables that drive C cycling. Roughness, our landscape level metric of permafrost thaw, captured the variation in microtopography of each wind direction sampled by the EC tower (Figure 1). We found that as microtopography decreased (ground became more subsided), active layer depths (ALD) increased, exponentially increasing after a threshold (Figure 2a). This pattern is a result of changes in soil thermal conductivity created by the redistribution of water into subsided areas, which increases soil temperature within depressions while decreasing temperatures in higher, dryer areas [*Jorgenson et al.*, 2001; *Kane et al.*, 2001; *Osterkamp et al.*, 2009]. These physical changes in soil moisture and temperature drive variable depths of thaw across the hillslope. This landscape level pattern of ALD and subsidence is consistent with previous work at this site, which showed similar relationships between microtopography, temperature, and moisture [*Lee et al.*, 2011; *Vogel et al.*, 2009].

[36] Areas with greater roughness had higher mean NDVI, with NDVI increasing with roughness until a threshold was reached (Figure 2b). Unlike ALD, NDVI leveled out and slightly decreased at the upper end of the roughness scale.

NDVI has been shown to be positively correlated with leaf area index [*Tucker*, 1979; *Williams et al.*, 2008], aboveground biomass [*Boelman et al.*, 2003; *Sellers*, 1985], net primary production [*Goward et al.*, 1985], GPP and R_{eco} [*Boelman et al.*, 2003; *La Puma et al.*, 2007; *Vourlitis et al.*, 2003]. Permafrost thaw within the EML watershed causes a shift in species composition from a plant community dominated by tussock-forming sedges to a community with increased shrub and moss abundance, and concurrently an increase in biomass and productivity [*Schuur et al.*, 2007; *Vogel et al.*, 2009]. Our result of increased NDVI with increased roughness is consistent with this pattern of increased biomass and productivity with thaw and also indicates that an upper limit of productivity may be reached as permafrost thaw continues and plants respond to the changing conditions. This upper limit is likely driven by the size of shrub species currently at the site, but could increase in the future, on the time scale of plant succession, if boreal trees were to increase in abundance at this tundra site.

[37] These relationships between microtopography and important biophysical features of the landscape (ALD and NDVI) highlight the feasibility of using remotely sensed spatial information to improve estimates of regional C balance in high-latitude ecosystems. Recent advancements in sensor resolution (e.g., LIDAR) now make microtopographical mapping of these vast, remote areas possible.

4.2. Incorporating Spatial Heterogeneity Into EC C Estimates

[38] We incorporated the spatial variability of C flux into the EC estimate of C exchange during gap filling using generalized additive models (GAMs). Because a continuous time series is required to estimate C balance, missing time periods must be modeled [*Baldocchi*, 2003; *Falge et al.*, 2001]. This gap-filling step provided a method for predicting C exchange based on the roughness of the landscape in specific wind directions, as well as more accurately determining the C balance of the entire landscape. We found that GAMs were equivalent or superior to traditional NL regression approaches (Table 1). GAMs had higher predictive power and a higher or equivalent coefficient of variation (R^2) than the NL models during all time periods. During cross validation, GAMs consistently had lower RMSE than NL models over all time periods, but were statistically lower only during GS days. The lack of statistical improvement in RMSE during GS nights and winter by the GAMs is not surprising because these time periods are notoriously difficult to model using any procedure [*Baldocchi*, 2003]. Overall, our model comparison to the more traditionally used NL gap-filling models gave us confidence that adding model complexity to include spatial information was justified.

[39] The aggregated predictions of C exchange from the GAM and NL models did not substantially differ from one another throughout either 2008 or 2009 (Figure 4). However, there were notable time periods where the two methods diverged in their predictive capabilities. During the early growing season of 2008 (weeks 21–29), the GAM substantially overpredicted R_{eco} compared to the NL model (Figure 4b). We believe this difference is due to a lack of data during the early GS, which caused the GAM to miss the

upswing of R_{eco} that coincides with rapid changes in phenology during the spring. Predictions of R_{eco} and NEE from the NL and GAM also diverged during the transition from the GS to winter in 2008, and the transition from the winter to the GS of 2009 (Figures 4b and 4c). We attributed this sensitivity to seasonal transitions by the GAM to the flexibility of their smoothing functions, which can capture rapidly changing trends in the data [*Zuur et al.*, 2009]. Because the NL models' empirically derived parameter estimates depend on relationships that change dramatically in this highly seasonal ecosystem, the relationships would need to be continuously updated in order to capture these transitions [*Baldocchi*, 2003; *Falge et al.*, 2001]. Biologically, the dip in R_{eco} during the transition in and out of winter could be attributed to changes in microbial species composition, or to the disruption of biological activity by the state change (freezing point) of water [*Mikan et al.*, 2002; *Rivkina et al.*, 2000]. This dip in R_{eco} could also be caused by shifts in the availability and use of substrates by microbes between the GS and winter [*Davidson and Janssens*, 2006; *Dioumaeva et al.*, 2002; *Hobbie et al.*, 2000].

4.3. Effects of Spatial Heterogeneity on C Flux

[40] By incorporating spatial information, we were able to estimate the C balance of the landscape in two different ways. First, we filled gaps depending on the measured wind direction at the time of the gap and created a single time series of C exchange for the entire landscape (GAM 1). Second, we gap filled the entire time series for each wind direction separately and averaged the predictions to estimate the C balance of the landscape (GAM 360). This allowed us to estimate C exchange for the entire heterogeneous landscape and also make predictions for the wind directions with the minimum and maximum roughness. Final C estimates from GAM 1 and GAM 360 were nearly identical (Figure 4). This similarity indicates that the wind distribution sampled by the EC tower was sufficient to capture the variability of thaw seen across the entire radial landscape surrounding the tower.

[41] The landscape on average (GAM 360) was a C sink during both 6 month measurement campaigns. The wind direction with the most variation in microtopography (maximum roughness), resulting from permafrost thaw and ground subsidence, had both higher GPP and R_{eco} than the landscape on average (Figures 5a and 5b), while the wind direction with least variation (minimum roughness) exhibited lower GPP and lower R_{eco}. Overall, during the 6 month campaign of 2008, the area with highest roughness gained 55.2% more C than the landscape on average, while the area with lowest roughness gained 76.4% less C. Similarly, during the 6 month campaign of 2009, the area with the highest roughness gained 41.4% more C, while the areas with lowest roughness gained 61.7% less C (Table 2). On the basis of these results, permafrost thaw and ground subsidence amplifies both GPP and R_{eco}.

[42] The amplification of GPP with roughness was consistent throughout the GS of both 2008 and 2009 (Figures 3 and 5a). This enhanced C sequestration could be due to shifts in the plant community to more highly productive species as permafrost thaws [*Osterkamp et al.*, 2009; *Schuur et al.*, 2007], or to increased plant productivity due to greater

nutrient availability resulting from enhanced decomposition within subsided areas [*Mack et al.*, 2004; *Shaver et al.*, 1992; *Vogel et al.*, 2009; *Natali et al.*, 2012]. Our results of higher NDVI in areas with higher roughness also support the idea of increased productivity as permafrost thaws (Figure 2b), as do several other studies that show NDVI is positively correlated with both R_{eco} and GPP [*Boelman et al.*, 2003; *La Puma et al.*, 2007; *Vourlitis et al.*, 2003].

[43] Ecosystem respiration also increased in areas of the landscape with greater roughness during the GS of both years (Figures 3 and 5b) because of greater temperature and moisture associated with greater ALD (Figure 2a) [*Lee et al.*, 2011; *Vogel et al.*, 2009]. More organic C is exposed to above freezing temperatures as ALD increases. These abiotic changes stimulate decomposition and nitrogen mineralization, which result in increased heterotrophic respiration [*Shaver et al.*, 1992]. *Vogel et al.* [2009] found that as subsidence increased, ALD increased and, in conjunction, both GPP and R_{eco} increased. These results are consistent with a large body of work showing that temperature and moisture are often the major determinates of organic matter decomposition and ecosystem respiration [*Davidson and Janssens*, 2006; *Davidson et al.*, 1998; *Hobbie et al.*, 2000; *Oberbauer et al.*, 1991; *Shaver et al.*, 1992; *Xu and Qi*, 2001]. There is also increased autotrophic respiration from more highly productive plants in subsided areas contributing to the overall increase in R_{eco} during the GS [*Schuur et al.*, 2007; *Vogel et al.*, 2009].

[44] In contrast to the GS, areas with increased roughness had lower C emissions during the winter (Figures 3 and 5b). Even though areas with less roughness had higher R_{eco} during winter, the overall C emission throughout 2008 and 2009 was still greater from areas with highest roughness. The reversal of the relationship of roughness and R_{eco} during the winter is opposite previous work at the site that estimated more subsided areas have greater C emissions [*Vogel et al.*, 2009]. They attributed greater winter C flux from subsided areas to warmer soils resulting from delayed active layer refreezing and the added insulation from snow accumulating in subsided areas, but data in the critical winter months was admittedly scarce [*Hinkel and Hurd*, 2006; *Vogel et al.*, 2009]. The inconsistency of our data may be due to differential diffusion through variations in snow cover trapped in subsided areas. The coefficient of variation of the top GAM was also very low, only 0.16 and 0.22 during winter of 2008 and 2009, respectively. Overall, there was little variation in winter C flux (throughout space or time) and we believe more measurements are needed before our winter pattern can be fully supported. More winter data is also crucial for determining the ecosystem's annual C balance and its feedback to climate change.

5. Conclusions

[45] We estimated the C balance of a heterogeneous landscape undergoing permafrost thaw by incorporating spatial variation into an eddy covariance estimate. We found strong relationships between thaw induced ground subsidence and ALD and NDVI, which both correlate with C flux. These microtopographical changes also strongly correlated with NEE. By using GAMs, we incorporated these

spatial relationships back into final EC C balance estimates during gap filling. Thus, we achieved a more accurate C estimate for the heterogeneous landscape and could make predictions for areas undergoing various degrees of permafrost thaw. Using GAMs, we were better able to predict C exchange during seasonal transitions, which indicates this type of gap-filling strategy would be good in systems with high temporal variability. Because all natural ecosystems vary through space and time, we believe GAMs can be an important tool for achieving more accurate C estimates. The use of GAMs will also allow EC towers to be placed in more heterogeneous environments than they have been previously used.

[46] As permafrost thaws within this upland tundra ecosystem, a heterogeneous environment is created by changes in microtopography. We found this ecosystem was a C sink during 2 consecutive years, and areas with greater thaw exhibited greater C sequestration (GPP) and greater C loss (R_{eco}). Thawing of permafrost increases the amplitude of the C cycle, which has important implications for the future landscape-level C balance [*Zimov et al.*, 1996]. Currently, GPP is stimulated more than R_{eco}, but this balance may shift because we found that NDVI diminished with increased permafrost thaw indicating there may be an upper limit in productivity, unless successional changes in vegetation occur.

[47] Although we found the ecosystem was a C sink during the measurement campaigns of both years, this is not representative of the annual C balance. We did not measure C flux during a portion of the winter season, and even though C fluxes during this time period are relatively low, the length of the season make it very important. By linearly extrapolating between these missing winter periods, we found that annually the ecosystem became a C source of 60 g C m^{-2} yr^{-1} and 13 g C m^{-2} yr^{-1} in 2008 and 2009, respectively.

References

Anderson, D. R., K. P. Burnham, and G. C. White (1998), Comparison of Akaike information criterion and consistent Akaike information criterion for model selection and statistical inference from capture-recapture studies, *J. Appl. Stat.*, 25, 263–282, doi:10.1080/02664769823250.

Anderson, D. R., K. P. Burnham, and G. C. White (2001), Kullback-Leibler information in resolving natural resource conflicts when definitive data exist, *Wildlife Soc. Bull.*, 29, 1260–1270.

Anisimov, O., and F. Nelson (1996), Permafrost distribution in the Northern Hemisphere under scenarios of climatic change, *Global Planet. Change*, 14, 59–72, doi:10.1016/0921-8181(96)00002-1.

Aubinet, M., et al. (1999), Estimates of the annual net carbon and water exchange of forests: The EUROFLUX methodology, *Adv. Ecol. Res*, 30, 113–175, doi:10.1016/S0065-2504(08)60018-5.

Aubinet, M., B. Heinesch, and B. Longdoz (2002), Estimation of the carbon sequestration by a heterogeneous forest: Night flux corrections, heterogeneity of the site and inter-annual variability, *Global Change Biol.*, 8, 1053–1071, doi:10.1046/j.1365-2486.2002.00529.x.

Baldocchi, D. (2003), Assessing the eddy covariance technique for evaluating carbon dioxide exchange rates of ecosystems: Past, present and future, *Global Change Biol.*, 9, 479–492, doi:10.1046/j.1365-2486.2003.00629.x.

Boelman, N., M. Stieglitz, H. Rueth, M. Sommerkorn, K. Griffin, G. Shaver, and J. Gamon (2003), Response of NDVI, biomass, and ecosystem gas exchange to long-term warming and fertilization in wet sedge tundra, *Oecologia*, 135, 414–421.

Burba, G. G., D. K. McDermitt, A. Grelle, D. J. Anderson, and L. K. Xu (2008), Addressing the influence of instrument surface heat exchange on the measurements of CO_2 flux form open-path gas analyzers, *Global Change Biol.*, 14, 1854–1876, doi:10.1111/j.1365-2486.2008.01606.x.

Chapin, F., III, W. Eugster, J. McFadden, A. Lynch, and D. Walker (2000), Summer differences among arctic ecosystems in regional climate forcing, *J. Clim.*, 13, 2002–2010, doi:10.1175/1520-0442(2000)013<2002:SDAAEI>2.0.CO;2.

Chapin, F., III, et al. (2005), Role of land-surface changes in arctic summer, *Science*, 310, 657–660, doi:10.1126/science.1117368.

Clark, K. L., H. L. Gholz, J. B. Moncrieff, F. Cropley, and H. W. Loescher (1999), Environmental controls over net exchanges of carbon dioxide from contrasting Florida ecosystems, *Ecol. Appl.*, 9, 936–948, doi:10.1890/1051-0761(1999)009[0936:ECONEO]2.0.CO;2.

Davidson, E., and I. Janssens (2006), Temperature sensitivity of soil carbon decomposition and feedbacks to climate change, *Nature*, 440, 165–173, doi:10.1038/nature04514.

Davidson, E., E. Belk, and R. Boone (1998), Soil water content and temperature as independent or confounded factors controlling soil respiration in a temperate mixed hardwood forest, *Global Change Biol.*, 4, 217–227, doi:10.1046/j.1365-2486.1998.00128.x.

Dioumaeva, I., S. Trumbore, E. Schuur, M. Goulden, M. Litvak, and A. Hirsch (2002), Decomposition of peat from upland boreal forest: Temperature dependence and sources of respired carbon, *J. Geophys. Res.*, 107, 8222, doi:10.1029/2001JD000848. [Printed 108(D3), 2003.]

Dormann, C. F. (2007), Effects of incorporating spatial autocorrelation into the analysis of species distribution data, *Global Ecol. Biogeogr.*, 16, 129–138, doi:10.1111/j.1466-8238.2006.00279.x.

Falge, E., D. Baldocchi, R. Olson, P. Anthoni, M. Aubinet, C. Bernhofer, G. Burba, R. Ceulemans, R. Clement, and H. Dolman (2001), Gap filling strategies for defensible annual sums of net ecosystem exchange, *Agric. For. Meteorol.*, 107, 43–69, doi:10.1016/S0168-1923(00)00225-2.

Goulden, M., J. Munger, S. Fan, B. Daube, and S. Wofsy (1996), Measurements of carbon sequestration by long-term eddy covariance: Methods and a critical evaluation of accuracy, *Global Change Biol.*, 2, 169–182, doi:10.1111/j.1365-2486.1996.tb00070.x.

Goward, S., C. Tucker, and D. Dye (1985), North American vegetation patterns observed with the NOAA-7 advanced very high resolution radiometer, *Vegetation*, 64, 3–14, doi:10.1007/BF00033449.

Hastie, T. J., and R. J. Tibshirani (1990), *Generalized Additive Models*, Chapman and Hall, Boca Raton, Fla.

Hicks Pries, C., E. Schuur, and K. Crummer (2011), Holocene carbon stocks and carbon accumulation rates altered in soils undergoing permafrost thaw, *Ecosystems*, 15, 162–173, doi:10.1007/s10021-011-9500-4.

Hinkel, K. M., and J. K. Hurd (2006), Permafrost destabilization and thermokarst following snow fence installation, Barrow, Alaska, USA, *Arct. Antarct. Alp. Res.*, 38, 530–539, doi:10.1657/1523-0430(2006)38[530:PDATFS]2.0.CO;2.

Hinzman, L., N. Bettez, W. Bolton, F. Chapin, M. Dyurgerov, C. Fastie, B. Griffith, R. Hollister, A. Hope, and H. Huntington (2005), Evidence and implications of recent climate change in northern Alaska and other arctic regions, *Clim. Change*, 72, 251–298, doi:10.1007/s10584-005-5352-2.

Hobbie, S., J. Schimel, S. Trumbore, and J. Randerson (2000), Controls over carbon storage and turnover in high-latitude soils, *Global Change Biol.*, 6, suppl. 1, 196–210, doi:10.1046/j.1365-2486.2000.06021.x.

Hollinger, D. Y., F. M. Kelliher, J. N. Byers, J. E. Hunt, T. M. Mcseveny, and P. L. Weir (1994), Carbon-dioxide exchange between an undisturbed old-growth temperate forest and the atmosphere, *Ecology*, 75, 134–150, doi:10.2307/1939390.

Intergovenmental Panel on Climate Change (2007), *Climate Change 2007: The Physical Science Basis: Working Group 1 Contribution to the Fourth Assessment Report of the Intergovernmental Panel on Climate Change*, edited by S. Solomon et al., 996 pp., Cambridge Univ. Press, New York.

Jorgenson, M., and T. Osterkamp (2005), Response of boreal ecosystems to varying modes of permafrost degradation, *Can. J. For. Res.*, *35*, 2100–2111, doi:10.1139/x05-153.

Jorgenson, M., C. Racine, J. Walters, and T. Osterkamp (2001), Permafrost degradation and ecological changes associated with a warming climate in central Alaska, *Clim. Change*, *48*, 551–579, doi:10.1023/A:1005667424292.

Kane, D., K. Hinkel, D. Goering, L. Hinzman, and S. Outcalt (2001), Nonconductive heat transfer associated with frozen soils, *Global Planet. Change*, *29*, 275–292, doi:10.1016/S0921-8181(01)00095-9.

Kim, Y. J., and C. Gu (2004), Smoothing spline Gaussian regression: More scalable computation via efficient approximation, *J. R. Stat. Soc., Ser. B*, *66*, 337–356, doi:10.1046/j.1369-7412.2003.05316.x.

Kljun, N., R. Kormann, N. Rotach, and F. Meixner (2003), Comparison of the Langrangian footprint model LPDM-B with an analytical footprint model, *Boundary Layer Meteorol.*, *106*, 349–355, doi:10.1023/A:1021141223386.

Kormann, R., and F. Meixner (2001), An analytical footprint model for non-neutral stratification, *Boundary Layer Meteorol.*, *99*, 207–224, doi:10.1023/A:1018991015119.

Laine, A., M. Sottocornola, G. Kiely, K. Byrne, D. Wilson, and E. Tuittila (2006), Estimating net ecosystem exchange in a patterned ecosystem: Example from blanket bog, *Agric. For. Meteorol.*, *138*, 231–243, doi:10.1016/j.agrformet.2006.05.005.

La Puma, I., T. Philippi, and S. Oberbauer (2007), Relating NDVI to ecosystem CO_2 exchange patterns in response to season length and soil warming manipulations in arctic Alaska, *Remote Sens. Environ.*, *109*, 225–236, doi:10.1016/j.rse.2007.01.001.

Lawrence, D., A. Slater, V. Romanovsky, and D. Nicolsky (2008), Sensitivity of a model projection of near-surface permafrost degradation to soil column depth and representation of soil organic matter, *J. Geophys. Res.*, *113*, F02011, doi:10.1029/2007JF000883.

Lee, H., E. Schuur, J. Vogel, M. Lavoie, D. Bhadra, and C. Staudhammer (2011), A spatially explicit analysis to extrapolate carbon fluxes in upland tundra where permafrost is thawing, *Global Change Biol.*, *17*, 1379–1393, doi:10.1111/j.1365-2486.2010.02287.x.

Liebethal, C., and T. Foken (2007), Evaluation of six parameterization approaches from the ground heat flux, *Theor. Appl. Climatol.*, *88*, 43–56, doi:10.1007/s00704-005-0234-0.

Liebethal, C., B. Huwe, and T. Foken (2005), Sensitivity analysis for two ground heat flux calculation approaches, *Agric. For. Meteorol.*, *132*, 253–262, doi:10.1016/j.agrformet.2005.08.001.

Mack, M., E. Schuur, M. Bret-Harte, G. Shaver, and F. Chapin III (2004), Ecosystem carbon storage in arctic tundra reduced by long-term nutrient fertilization, *Nature*, *431*, 440–443, doi:10.1038/nature02887.

Mikan, C., J. Schimel, and A. Doyle (2002), Temperature controls of microbial respiration in arctic tundra soils above and below freezing, *Soil Biol. Biochem.*, *34*, 1785–1795, doi:10.1016/S0038-0717(02)00168-2.

Moncrieff, J. B., J. M. Massheder, H. deBruin, J. Elbers, T. Friborg, B. Heusinkveld, P. Kabat, S. Scott, H. Soegaard, and A. Verhoef (1997), A system to measure surface fluxes of momentum, sensible heat, water vapour and carbon dioxide, *J. Hydrol.*, *188–189*, 589–611, doi:10.1016/S0022-1694(96)03194-0.

Natali, S. M., E. A. G. Schuur, and R. L. Rubin (2012), Increased plant productivity in Alaskan tundra with experimental warming of soil and permafrost, *Ecology*, doi:10.1111/j.1365-2745.2011.01925.x, in press.

Oberbauer, S., J. Tenhunen, and J. Reynolds (1991), Environmental effects on CO_2 efflux from water track and tussock tundra in arctic Alaska, USA, *Arct. Alp. Res.*, *23*, 162–169, doi:10.2307/1551380.

Osterkamp, T., M. Jorgenson, E. Schuur, Y. Shur, M. Lamevskiy, J. Vogel, and V. Tumskoy (2009), Physical and ecological changes associated with warming permafrost and thermokarst in interior Alaska, *Permafrost Periglacial Processes*, *20*, 235–256, doi:10.1002/ppp.656.

R Development Core Team (2010), *R: A Language and Environment for Statistical Computing*, R Found. for Stat. Comput., Vienna.

Reynolds, O. (1895), On the dynamical theory of incompressible viscous fluids and the determination of the criterion, *Philos. Trans. R. Soc. London, Ser. A*, *186*, 123–164, doi:10.1098/rsta.1895.0004.

Richardson, A., M. Mahecha, E. Falge, J. Kattge, A. Moffat, D. Papale, M. Reichstein, V. Stauch, B. Braswell, and G. Churkina (2008), Statistical properties of random CO_2 flux measurement uncertainty inferred from model residuals, *Agric. For. Meteorol.*, *148*, 38–50, doi:10.1016/j.agrformet.2007.09.001.

Rivkina, E., E. Friedmann, C. McKay, and D. Gilichinsky (2000), Metabolic activity of permafrost bacteria below the freezing point, *Appl. Environ. Microbiol.*, *77*, 3230–3233.

Romanovsky, V., S. Gruber, A. Instanes, H. Jin, S. Marchenko, S. Smith, D. Trombotto, and K. Walter (2007), Frozen ground, in *Global Outlook*

for Ice and Snow, edited by U. N. Environ. Programme, pp. 181–200, Arendal, Norway.

Saito, K., M. Kimoto, T. Zhang, K. Takata, and S. Emori (2007), Evaluating a high-resolution climate model: Simulated hydrothermal regimes in frozen ground regions and their change under the global warming scenario, *J. Geophys. Res.*, *112*, F02S11, doi:10.1029/2006JF000577.

Schmid, H. (1997), Experimental design for flux measurements: Matching scales of observations and fluxes, *Agric. For. Meteorol.*, *87*, 179–200, doi:10.1016/S0168-1923(97)00011-7.

Schmid, H. (2002), Footprint modeling for vegetation atmosphere exchange studies: A review and perspective, *Agric. For. Meteorol.*, *113*, 159–183, doi:10.1016/S0168-1923(02)00107-7.

Schmid, H., and C. Lloyd (1999), Spatial representativeness and the location bias of flux footprints over inhomogeneous areas, *Agric. For. Meteorol.*, *93*, 195–209, doi:10.1016/S0168-1923(98)00119-1.

Schuur, E., K. Crummer, J. Vogel, and M. Mack (2007), Plant species composition and productivity following permafrost thaw and thermokarst in Alaskan tundra, *Ecosystems*, *10*, 280–292, doi:10.1007/s10021-007-9024-0.

Schuur, E., J. Bockheim, J. Canadell, E. Euskirchen, C. Field, S. Goryachkin, S. Hagemann, P. Kuhry, P. Lafleur, and E. Lee (2008), Vulnerability of permafrost carbon to climate change: Implications for the global carbon cycle, *BioScience*, *58*, 701–714, doi:10.1641/B580807.

Schuur, E., J. Vogel, K. Crummer, H. Lee, J. Sickman, and T. Osterkamp (2009), The effect of permafrost thaw on old carbon release and net carbon exchange from tundra, *Nature*, *459*, 556–559, doi:10.1038/nature08031.

Sellers, P. (1985), Canopy reflectance, photosynthesis and transpiration. Part II. The role of biophysics in the linearity of their interdependance, *Int. J. Remote Sens.*, *6*, 1335–1372, doi:10.1080/01431168508948283.

Shaver, G., W. Billings, F. Chapin III, A. Giblin, K. Nadelhoffer, W. Oechel, and E. Rastetter (1992), Global change and the carbon balance of arctic ecosystems, *BioScience*, *42*, 433–441, doi:10.2307/1311862.

Soil Survey Staff (1999), *Soil Taxonomy: A Basic System of Soil Classification for Making and Interpreting Soil Surveys*, U.S. Govt. Print. Off., Washington, D. C.

Tarnocai, C., J. Canadell, G. Mazhitova, E. Schuur, P. Kuhry, and S. Zimov (2009), Soil organic carbon pools in the northern circumpolar permafrost region, *Global Biogeochem. Cycles*, *23*, GB2023, doi:10.1029/2008GB003327.

Thornley, J. H., and I. R. Johnson (1990), *Plant and Crop Modeling: A Mathematical Approach to Plant and Crop Physiology*, Charldon, Oxford, U. K.

Tucker, C. (1979), Red and photographic infrared linear combinations for monitoring vegetation, *Remote Sens. Environ.*, *8*, 127–150, doi:10.1016/0034-4257(79)90013-0.

Venables, W., and B. Ripley (2002), *Modern Applied Statistics With S*, 4th ed., Springer, New York.

Vogel, J., E. Schuur, C. Trucco, and H. Lee (2009), Response of CO_2 exchange in a tussock tundra ecosystem to permafrost thaw and thermokarst development, *J. Geophys. Res.*, *114*, G04018, doi:10.1029/2008JG000901.

Vourlitis, G., J. Verfaillie, W. Oechel, A. Hope, D. Stow, and R. Engstrom (2003), Spatial variation in regional CO_2 exchange for the Kuparuk River Basin, Alaska over the summer growing season, *Global Change Biol.*, *9*, 930–941, doi:10.1046/j.1365-2486.2003.00639.x.

Webb, E. K., G. I. Pearman, and R. Leuning (1980), Correction of flux measurements for density effects due to heat and water-vapor transfer, *Q. J. R. Meteorol. Soc.*, *106*, 85–100, doi:10.1002/qj.49710644707.

Wilczak, J., S. Oncley, and S. Stage (2001), Sonic anemometer tilt correction algorithms, *Boundary Layer Meteorol.*, *99*, 127–150, doi:10.1023/A:1018966204465.

Williams, M., R. Bell, L. Spadavecchia, E. Street, and M. Van Wijk (2008), Upscaling leaf area index in an arctic landscape through multiscale observations, *Global Change Biol.*, *14*, 1517–1530, doi:10.1111/j.1365-2486.2008.01590.x.

Wood, S. (2006), *Generalized Additive Models: An Introduction With R*, Chapman and Hall, Boca Raton, Fla.

Wood, S. N. (2008), Fast stable direct fitting and smoothness selection for generalized additive models, *J. R. Stat. Soc., Ser. B*, *70*, 495–518, doi:10.1111/j.1467-9868.2007.00646.x.

Xu, M., and Y. Qi (2001), Soil-surface CO_2 efflux and its spatial and temporal variations in a young ponderosa pine plantation in northern California, *Global Change Biol.*, *7*, 667–677, doi:10.1046/j.1354-1013.2001.00435.x.

Yocum, L. C., G. W. Adema, and C. K. Hults (2006), *A Baseline Study of Permafrost in the Totlat Basin*, Denali Natl. Park and Preserve, Denali Park, Alaska.

Zhang, T., R. Barry, K. Knowles, J. Heginbottom, and J. Brown (1999), Statistics and characteristics of permafrost and ground-ice distribution in the Northern Hemisphere, *Polar Geogr.*, *23*, 132–154, doi:10.1080/10889379909377670.

Zhang, T., O. Frauenfeld, M. Serreze, A. Etringer, C. Oelke, J. McCreight, R. Barry, D. Gilichinsky, D. Yang, and H. Ye (2005), Spatial and temporal variability in active layer thickness over the Russian arctic drainage basin, *J. Geophys. Res.*, *110*, D16101, doi:10.1029/2004JD005642.

Zimov, S., S. Davidov, Y. Voropaev, S. Prosiannikov, I. Semiletov, M. Chapin, and F. Chapin (1996), Siberian CO_2 efflux in winter as a CO_2 source and cause of seasonality in atmospheric CO_2, *Clim. Change*, *33*, 111–120, doi:10.1007/BF00140516.

Zuur, A., E. Ieno, N. Walker, A. Saveliev, and G. Smith (2009), *Mixed Effects Models and Extensions in Ecology With R*, Springer, New York.

E. F. Belshe, R. Bracho, and E. A. G. Schuur, Department of Biology, University of Florida, 220 Bartrum-Carr Hall, PO Box 118525, Gainesville, FL 32611, USA. (fayray@ufl.edu)

B. M. Bolker, Department of Mathematics and Statistics, McMaster University, 314 Hamilton Hall, 1280 Main St. W., Hamilton, ON L8S 4K1, Canada.